

# Critical-Current Measurements on an ITER Nb<sub>3</sub>Sn Strand: Effect of Axial Tensile Strain

Najib Cheggour, Jack W. Ekin, and Loren F. Goodrich

**Abstract**—The dependence of transport critical current ( $I_c$ ) on axial tensile strain  $\varepsilon$  was measured for a developmental Nb<sub>3</sub>Sn multifilamentary strand as a function of magnetic field  $B$  between 12 T and 16 T, at the temperature of 4 K. This conductor was from the first stage of strand pre-production for the central solenoid of the International Thermonuclear Experimental Reactor (ITER) project. Straight samples were measured with a stress-free-cooling strain apparatus. The compressive pre-strain  $\varepsilon_{\max}$  and the irreversible strain limit  $\varepsilon_{\text{irr}}$  were 0.19% and 0.8%, respectively; and the ultimate strain where the wire physically broke was about 0.95%. The pinning force  $F_p (= I_c \times B)$  was proportional to  $(B_{c2}^*)^s b^p (1 - b)^q$ , where  $b = B/B_{c2}^*$  is the reduced magnetic field, and the scaling constants had values  $p = 0.58$ ,  $q = 1.86$ , and  $s = 0.7$ . The strain dependence of the effective upper critical field  $B_{c2}^*$  (the field at which  $F_p$  extrapolates to zero) was well described within the measured strain range by  $B_{c2, \max}^* [1 - a|\varepsilon - \varepsilon_{\max}|^u]$ , where  $B_{c2, \max}^*$  is the maximum value of  $B_{c2}^*$  as a function of strain,  $u = 1.7$ , and  $a$  was about 1230 for the compressive strains and 1670 for the tensile strains. Ekin's strain scaling law was applied to calculate the strain sensitivity of  $I_c$  at various intrinsic strains between  $-0.5\%$  and  $0.5\%$ , and magnetic fields from 12 T to 16 T.

**Index Terms**—Axial strain, critical current, ITER, niobium-tin, pinning force, stress-free cooling, superconductor magnet.

## I. INTRODUCTION

NIObIUM-TIN (Nb<sub>3</sub>Sn) superconductor strands to be used in the International Thermonuclear Experimental Reactor (ITER) will be subjected to enormous mechanical forces, which will influence the conductor transport properties. This is especially true due to the relatively high sensitivity of Nb<sub>3</sub>Sn compound to strain [1]. Therefore, a full characterization of the dependence on strain of the strand critical current ( $I_c$ ) is crucial to better predict the behavior of the conductor under the severe operating conditions of the ITER.

In this work, we measured the effect of axial strain at 4 K in one of the developmental Nb<sub>3</sub>Sn multifilamentary wires of the first stage of strand pre-production for the ITER central solenoid. In particular, we determined the shape of the pinning force  $F_p (= I_c \times B)$  versus magnetic field  $B$  and strain  $\varepsilon$ , and the dependence on strain of the effective upper critical field  $B_{c2}^*$  at which  $F_p$  extrapolates to zero. We also determined the compressive pre-strain  $\varepsilon_{\max}$  where the  $I_c(\varepsilon)$  and  $B_{c2}^*(\varepsilon)$  curves reach

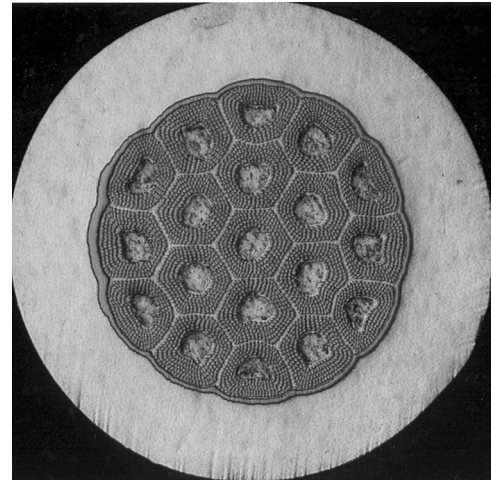


Fig. 1. Micrograph of a developmental multifilamentary Nb<sub>3</sub>Sn wire for the ITER central solenoid (courtesy of T. Pyon, Luvata Waterbury Inc.).

their maximum, and the irreversible strain limit  $\varepsilon_{\text{irr}}$  where mechanical cracks start to develop in the brittle Nb<sub>3</sub>Sn filaments. These results also complement the variable-temperature data obtained on the same wire (Specimen B in Reference [2]).

## II. EXPERIMENTAL PROCEDURE

### A. Strand Characteristics

The conductor, made by Luvata Waterbury Inc., included Ti as an additive, and had 19 subelements (Fig. 1), a diameter of 0.83 mm, a Cu to non-Cu ratio of 1.1, and a twist pitch of 12 mm. Sections of this wire were put inside quartz tubes with a close-fit inner diameter in order to keep the samples as straight as possible after they had undergone the reaction heat treatment. Samples measured in this work were reacted at 650 °C for 175 hours, preceded by a dwell at 575 °C for 100 hours to favor Sn migration toward Nb filaments. The heat-treatment duration was relatively short in order to keep ac losses within ITER specifications. Recently, longer heat treatments were used on the same conductor, which improved  $I_c$  values by about 19% and increased ac losses by only 4% with respect to the shorter annealing [3]. Hence the critical-current data presented here are not the optimum values for this particular strand. Three specimens were studied as a function of strain in liquid helium at 4 K. Samples #1 and #2 were measured at 15 T. Sample #3, which was Cu-plated for better stability, was measured in increasing magnetic fields from 12 T to 16 T.

Manuscript received August 29, 2006. This work was supported in part by the U.S. Department of Energy, Office of Fusion Energy Sciences, under Grant DE-FC02-93ER54186.

The authors are with the National Institute of Standards and Technology, Boulder, CO 80305 USA (e-mail: cheggour@boulder.nist.gov).

Digital Object Identifier 10.1109/TASC.2007.897819

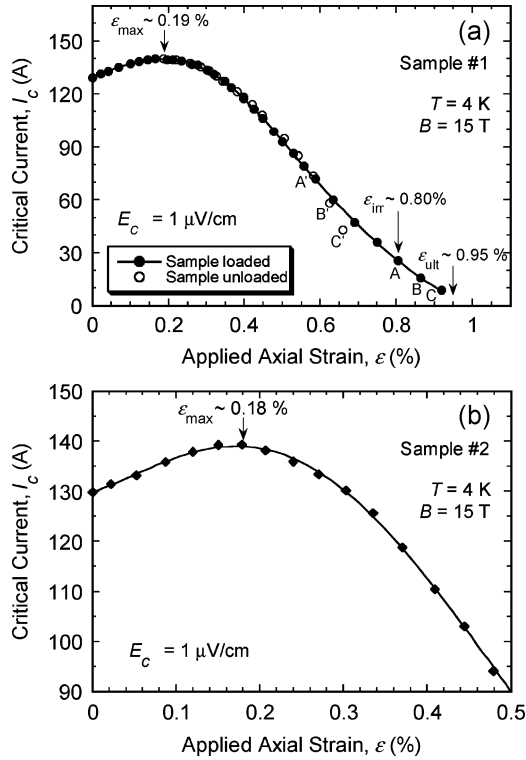


Fig. 2. Critical current as a function of applied axial strain at 4 K and 15 T, in a developmental Nb<sub>3</sub>Sn multifilamentary wire for the ITER central solenoid. Results were obtained for the non-Cu-plated samples #1 (a) and #2 (b). Open symbols in (a) represent values of critical current after unloading stress, which were used to determine the irreversible strain limit  $\epsilon_{\text{irr}}$ .

### B. Axial-Strain Apparatus

Measurements were made with a stress-free-cooling apparatus [4]. The ends of the sample were soldered to two Cu grips, which were also used as current contacts. A pair of voltage taps was attached to the sample's middle section. A calibrated extensometer was positioned between the two grips and measured the strain  $\epsilon$  applied to the specimen. The uncertainty in measurements of strain was about  $\pm 0.03\%$ .

Samples mounted on this apparatus had to be cut to short lengths of only 35 mm. The voltage-tap separation was typically about 3 mm to 7 mm. This left a distance between a current contact and its closest voltage tap of less than 10 mm, which was not enough to prevent current-transfer voltages for the samples measured in this work.

Current-transfer voltages make it difficult to obtain a direct determination of  $I_c$  values. To circumvent this problem, we measured voltage vs. current ( $V-I$ ) curves up to very high electric fields ( $100 \mu\text{V}/\text{cm}$ ) and back-extrapolated the  $I_c$  values as described in Reference [5]. Comparison of the extrapolated  $I_c$  values with data obtained with a different apparatus on a long sample of the same wire (with no current-transfer voltages) [2] showed fairly good agreement. Critical currents were determined at an electrical-field criterion  $E_c$  of  $1 \mu\text{V}/\text{cm}$ . Uncertainty in estimation of  $I_c$  values was about 5%.

We were able to use the back-extrapolation technique for samples #1 and #2 at 15 T and above, where  $I_c$  values were not too high, and  $V-I$  curves could be measured to high enough

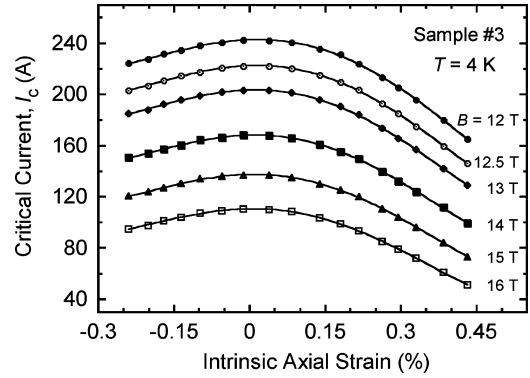


Fig. 3. Critical current as a function of intrinsic axial strain and magnetic field at 4 K, in a developmental Nb<sub>3</sub>Sn multifilamentary wire for the ITER central solenoid. Results were obtained for the Cu-plated sample #3.

electric-fields for satisfactory extrapolations. To allow measurements below 15 T, additional Cu had to be electroplated onto sample #3 in order to prevent sample quenching when an attempt was made to reach high electric-fields at high currents. Cu-plating changes the sample's compressive pre-strain  $\epsilon_{\text{max}}$  [6]. However, this was not a concern since  $\epsilon_{\text{max}}$  was determined from the measurements of the non-Cu-plated samples #1 and #2.

## III. RESULTS AND DISCUSSION

### A. Characteristic Strains

Critical current vs. strain results obtained at 4 K and 15 T on the non-Cu-plated samples #1 and #2 are depicted in Fig. 2.  $I_c$  reached a peak value at  $\epsilon_{\text{max}} \approx 0.19\%$ , corresponding to the amount of pre-compression exerted on Nb<sub>3</sub>Sn filaments when the samples were cooled from the heat-treatment temperature to 4 K [7], [8].  $\epsilon_{\text{max}}$  was similar for both samples.

For sample #1, measurements were made both when the specimen was strained and when strain was released in order to determine the irreversible strain limit  $\epsilon_{\text{irr}}$  where cracks start to form in the Nb<sub>3</sub>Sn filaments (Fig. 2a). When strain was released from strain point A (solid symbol), the position of the corresponding unloaded strain point A' (open symbol) showed that  $I_c$  vs.  $\epsilon$  behavior was still reversible. This reversibility ceased when the sample was strained beyond the strain point A. Hence the irreversible strain limit  $\epsilon_{\text{irr}} \approx 0.8\%$ . Subsequently, the sample physically broke at an ultimate strain  $\epsilon_{\text{ult}} \approx 0.95\%$ . The dependence on strain of the  $n$ -value (sharpness of the  $V-I$  curves) also yielded a determination of the irreversible strain limit  $\epsilon_{\text{irr}}$  close to 0.8%.

### B. Strain and Magnetic-Field Effects

Sample #3 was measured as a function of strain in increasing magnetic fields from 12 T to 16 T (Fig. 3). This sample was Cu-plated from its original diameter of 0.83 mm to a diameter of 1.02 mm. This was necessary to enable us make measurements in fields down to 12 T and 13 T (fields of interest to the ITER community), and cover enough field range to analyze the pinning force  $F_p(B, \epsilon)$  and extract the effective upper critical field  $B_{c2}^*(\epsilon)$ . In comparison to samples #1 and #2, the Cu plating of sample #3 artificially increased  $\epsilon_{\text{max}}$  to  $\approx 0.24\%$ . However, this increase does not alter the dependence of  $I_c$  on the intrinsic

strain ( $= \varepsilon - \varepsilon_{\max}$ ) of  $\text{Nb}_3\text{Sn}$  filaments [6]. The  $I_c$  results for sample #3 are plotted as a function of the intrinsic strain in Fig. 3. As expected, the  $I_c$  sensitivity to strain increased with field [9] (this point is clearer from normalized data in Fig. 5).

### C. Strain Scaling Law of the Pinning Force

Data were fitted with (1) to obtain the field dependence of the pinning force,

$$F_p = I_c \times B = K(\varepsilon) \left( \frac{B}{B_{c2}^*} \right)^p \left( 1 - \left( \frac{B}{B_{c2}^*} \right) \right)^q, \quad (1)$$

where  $K$  is a function of strain, and can be expressed in terms of the strain dependence of  $B_{c2}^*$  as [4]:

$$K(\varepsilon) \propto (B_{c2}^*(\varepsilon))^s. \quad (2)$$

In order to obtain optimum  $p$ ,  $q$ ,  $B_{c2}^*$  and  $K$  values, a code was written in *Microsoft Excel*, and a global least-square fit to the data was made using the subroutine *Solver* available with *Excel* [10], [11]. This procedure allows a more precise fit as compared to Kramer plots, where  $p$  and  $q$  are assumed to be equal to 0.5 and 2, respectively [12]. A minimum was found for  $p = 0.58$  and  $q = 1.86$ . Values of  $B_{c2}^*$  and  $K$  obtained from the global fit, and those obtained from fitting data of each strain point individually, were the same. Fig. 4a shows that the shape of  $F_p$  is invariant with strain, as formulated by Ekin's strain scaling law [4]. It is worth mentioning that  $p$  and  $q$  values are almost identical to those that fitted the variable-temperature data obtained on a sample of the same strand, heat-treated under the same conditions [2]. This confirms that  $p$  and  $q$  have little dependence on temperature and strain [10], [11], [13].

In Fig. 4b, the values of  $B_{c2}^*$  are plotted against the intrinsic strain. To parameterize the data, we used the expression introduced in [4]:

$$B_{c2}^*(\varepsilon, 4K) = B_{c2\max}^*(4K) (1 - a|\varepsilon - \varepsilon_{\max}|^u), \quad (3)$$

where  $B_{c2\max}^*$  is the peak value of  $B_{c2}^*$ ,  $a$  and  $u$  are fitting parameters.  $B_{c2\max}^* \approx 25.3$  T. Taking  $u = 1.7$  as in [4], the best fit was obtained with  $a = 1230$  for compressive strains ( $a-$ ), and  $a = 1670$  for tensile strains ( $a+$ ). These values are higher than those found for binary  $\text{Nb}_3\text{Sn}$  (i.e.  $a- = 900$ ,  $a+ = 1250$ ), confirming Ekin's reports for ternary and quaternary  $\text{Nb}_3\text{Sn}$  wires [14]. We used (3) to calculate  $B_{c2}^*$  for intrinsic strains between  $-0.5\%$  and  $0.5\%$ , as this expression is reported to be valid for at least this strain range [5] (results plotted in Fig. 4b). For very high compressive strain values beyond  $-0.5\%$ , the dependence of  $B_{c2}^*$  on intrinsic strain may present an upward curvature, and hence may deviate from (3) [11], [15].

The last parameter to find is the strain index  $s$  in (2). By plotting  $\log(F_{p\max})$  vs.  $\log(B_{c2}^*)$ , the slope  $s$  was  $\approx 0.7$ . With these fitting parameters, we now have the full expression of the strain scaling law (1) and (2), and can predict the effect of strain on  $I_c$  for various magnetic fields.

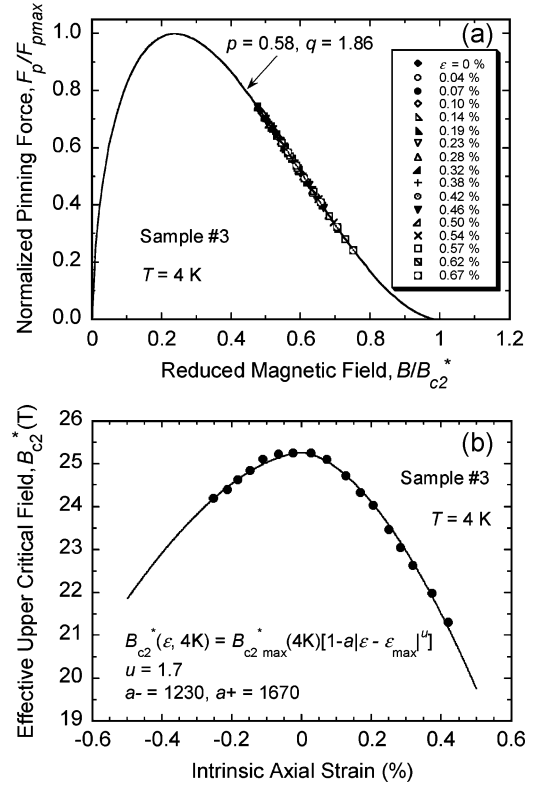


Fig. 4. Developmental  $\text{Nb}_3\text{Sn}$  multifilamentary wire for the ITER central solenoid. (a) Normalized pinning force as a function of reduced magnetic field at 4 K. The shape of the pinning force is invariant with strain. The continuous line is given by equation (1), with  $p = 0.58$  and  $q = 1.86$ . (b) Effective upper critical field as a function of intrinsic strain. The continuous line is a fitting function given by the expression shown in the figure (equation (3)).

### D. Application of the Strain Scaling Law

To predict the strain sensitivity of  $I_c$  at a given magnetic field, we used a known expression derived from the strain scaling law [4]:

$$\frac{I_c(B, \varepsilon)}{I_{c\max}(B)} = \left( \frac{B_{c2}^*(\varepsilon)}{B_{c2\max}^*} \right)^{s-p} \left( \frac{1 - B/B_{c2}^*(\varepsilon)}{1 - B/B_{c2\max}^*} \right)^q. \quad (4)$$

By combining this expression with (3), we calculated the ratio  $I_c/I_{c\max}$  at various intrinsic strains between  $-0.5\%$  and  $0.5\%$ , and magnetic fields from 12 T to 16 T. The results are presented in Table I, and are compared to the experimental data in Fig. 5. There is good agreement between the measured and calculated data. These calculations can provide useful engineering numbers for design purposes and for comparing between different strands candidates for the ITER project.

## IV. CONCLUSION

The strain scaling parameters were determined at 4 K for a developmental  $\text{Nb}_3\text{Sn}$  multifilamentary strand for the central solenoid of the ITER project. These parameters were  $p = 0.58$ ,  $q = 1.86$ ,  $u = 1.7$ ,  $a- = 1230$ ,  $a+ = 1670$ ,  $B_{c2\max}^* = 25.3$  T, and  $s = 0.7$ . Furthermore, the strand's characteristic strains were  $\varepsilon_{\max} = 0.19\%$ ,  $\varepsilon_{\text{irr}} = 0.8\%$ , and  $\varepsilon_{\text{ult}} = 0.95\%$ . By use of

TABLE I  
NORMALIZED CRITICAL CURRENT  $I_c/I_{c\max}$

$B$ (T)	Intrinsic strain (%)										
	-0.5	-0.4	-0.3	-0.2	-0.1	0	0.1	0.2	0.3	0.4	0.5
12	0.71	0.81	0.88	0.94	0.98	1	0.98	0.92	0.84	0.73	0.59
13	0.67	0.78	0.86	0.93	0.98	1	0.97	0.91	0.81	0.69	0.54
14	0.62	0.74	0.84	0.92	0.98	1	0.97	0.89	0.79	0.65	0.48
15	0.56	0.70	0.82	0.91	0.97	1	0.96	0.88	0.75	0.59	0.41
16	0.50	0.65	0.79	0.89	0.97	1	0.96	0.86	0.71	0.53	0.33

Ratio  $I_c/I_{c\max}$  for an ITER developmental Nb<sub>3</sub>Sn multifilamentary wire, calculated at various intrinsic strains between  $-0.5\%$  and  $0.5\%$ , and magnetic fields from 12 T to 16 T using equation (4). The fitting parameters were:  $p = 0.58$ ,  $q = 1.86$ ,  $u = 1.7$ ,  $a^- = 1230$ ,  $a^+ = 1670$ ,  $B_{c2\max}^* = 25.3$  T, and  $s = 0.7$ .

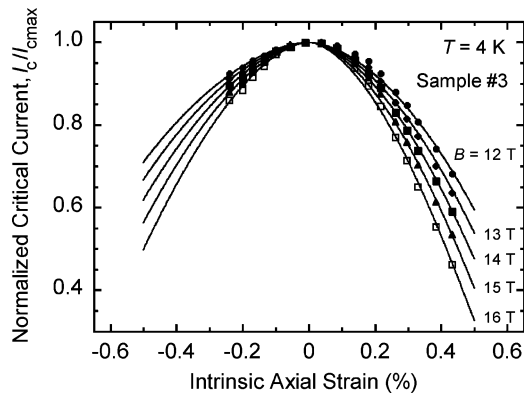


Fig. 5. Developmental Nb<sub>3</sub>Sn multifilamentary wire for the ITER central solenoid. Normalized critical current  $I_c/I_{c\max}$  at 4 K, as a function of intrinsic strain between  $-0.5\%$  and  $0.5\%$  and magnetic field from 12 T to 16 T. Experimental data (also shown not normalized in Fig. 3) are fitted with the expression in equation (4) derived from the strain scaling law [4]. The measured and calculated values are in good agreement.

the strain scaling law, calculations of the strain sensitivity of  $I_c$  at various magnetic fields showed good agreement with the experimental data points. These computations can provide useful engineering tools for design purposes and for strands comparisons.

#### ACKNOWLEDGMENT

The authors thank Dr. Joseph Minervini and his staff at the Massachusetts Institute of Technology, Plasma Science and Fusion Center, for their contributions and support of this research.

#### REFERENCES

[1] J. W. Ekin, "Strain effects in superconducting compounds," *Adv. Cryo. Eng.*, vol. 30, pp. 823–836, 1984.

- [2] L. F. Goodrich, N. Cheggour, J. W. Ekin, and T. C. Stauffer, "Critical-current measurements on ITER Nb<sub>3</sub>Sn strands: Effect of temperature," *IEEE Trans. Appl. Supercond.*, vol. 17, no. 2, 2006.
- [3] T. Pyon, J. Somerkoski, B. Karlemo, and M. Holm, "Development of high performance Nb<sub>3</sub>Sn conductor for fusion and accelerator application," *IEEE Trans. Appl. Supercond.*, vol. 17, no. 2, 2006.
- [4] J. W. Ekin, "Strain scaling law for flux pinning in practical superconductors. Part I: Basic relationship and application to Nb<sub>3</sub>Sn conductors," *Cryogenics*, vol. 20, pp. 611–624, 1980.
- [5] J. W. Ekin, *Experimental Techniques for Low Temperature Measurements*. UK: Oxford University Press, 2006.
- [6] J. W. Ekin, N. Cheggour, M. Abrecht, C. C. Clickner, M. Field, S. Hong, J. Parrell, and Y. Zhang, "Compressive pre-strain in high-niobium-fraction Nb<sub>3</sub>Sn superconductors," *IEEE Trans. Appl. Supercond.*, vol. 15, pp. 3560–3563, June 2005.
- [7] H. Hillmann, H. Kuckuck, H. Pfister, G. Rupp, E. Springer, M. Wilhelm, K. Wohlleben, and G. Ziegler, "Properties of multifilamentary Nb<sub>3</sub>Sn conductors," *IEEE Trans. Magn.*, vol. 13, pp. 792–795, 1977.
- [8] G. Rupp, "Enhancement of the critical current of multifilamentary Nb<sub>3</sub>Sn conductors by tensile stress," *J. Appl. Phys.*, vol. 48, pp. 3858–3863, 1977.
- [9] J. W. Ekin, "Effect of stress on the critical current of Nb<sub>3</sub>Sn multifilamentary composite wire," *Appl. Phys. Lett.*, vol. 29, pp. 216–219, August 1976.
- [10] N. Cheggour and D. P. Hampshire, "Unifying the strain and temperature scaling laws for the pinning force density in superconducting niobium-tin multifilamentary wires," *J. Appl. Phys.*, vol. 86, pp. 552–555, 1999.
- [11] N. Cheggour and D. P. Hampshire, "The unified strain and temperature scaling law for the pinning force density of bronze-route Nb<sub>3</sub>Sn wires in high magnetic fields," *Cryogenics*, vol. 42, pp. 299–309, 2002.
- [12] E. J. Kramer, "Scaling laws for flux pinning in hard superconductors," *J. Appl. Phys.*, vol. 44, pp. 1360–1370, 1973.
- [13] N. Cheggour and D. P. Hampshire, "Variable-temperature transport critical currents of niobium-tin wires under strain in high magnetic fields," *IEEE Trans. Appl. Supercond.*, vol. 9, pp. 2517–2520, June 1999.
- [14] J. W. Ekin, "High-field flux pinning and the strain scaling law," in *Proceedings of International Symposium on Flux Pinning and Electromagnetic Properties in Superconductors*, Fukuoka, Japan, 1985, pp. 267–271.
- [15] B. ten Haken, A. Godeke, and H. H. J. ten Kate, "The influence of compressive and tensile axial strain on the critical properties of Nb<sub>3</sub>Sn conductors," *IEEE Trans. Appl. Supercond.*, vol. 5, pp. 1909–1912, June 1995.